Received: 31 March 2018 | Revised: 12 April 2019 | Accepted: 5 May 2019

DOI: 10.1111/jbi.13642

RESEARCH PAPER

Journal of Biogeography | WILEY

# Dispersal kernels may be scalable: Implications from a plant pathogen

Daniel H. Farber[1] | Patrick De Leenheer[2] | Christopher C. Mundt[3]

[1]Department of Plant Pathology, Washington State University, Pullman, Washington

[2]Department of Mathematics, Oregon State University, Corvallis, Oregon

[3]Department of Botany and Plant Pathology, Oregon State University, Corvallis, Oregon

**Correspondence**
Daniel H. Farber, Department of Plant Pathology, Washington State University, Pullman, Washington.
Email: daniel.farber@wsu.edu

**Funding information**
National Science Foundation, Grant/Award Number: Ecology and Evolution of Infectious Diseases 05275; Oregon Agricultural Experiment Station; National Institute of Food and Agriculture, Grant/Award Number: 2015-67013-23818

Editor: Signe Normand

## Abstract

**Aim:** Understanding how spatial scale of study affects observed dispersal patterns can provide insights to spatiotemporal population dynamics, particularly in systems with significant long-distance dispersal (LDD). We aimed to investigate the dispersal gradients of two rusts of wheat with spores of similar size, mass and shape, over multiple spatial scales. We hypothesized that a single dispersal kernel could fit the dispersal from all spatial scales well, and that it would be possible to obtain similar results in spatiotemporal increase of disease when modelling based on differing scales.

**Location:** Central Oregon and St. Croix Island.

**Taxa:** *Puccinia striiformis* f. sp. *tritici*, *Puccinia graminis* f. sp. *tritici*, *Triticum aestivum*.

**Methods:** We compared empirically derived primary disease gradients of cereal rust across three spatial scales: local (inoculum source and sampling unit = 0.0254 m, spatial extent = 1.52 m) field-wide (inoculum source = 1.52 m, sampling unit = 0.305 m and spatial extent = 91.4 m) and regional (inoculum source and sampling unit = 152 m, spatial extent = 10.5 km). We then examined whether disease spread in spatially explicit simulations depended upon the scale at which data were collected by constructing a compartmental time-step model.

**Results:** The three data sets could be fit well by a single power law dispersal kernel. Simulating epidemic spread at different spatial resolutions resulted in similar patterns of spatiotemporal spread. Dispersal kernel data obtained at one spatial scale can be used to represent spatiotemporal disease spread at a larger spatial scale.

**Main Conclusions:** Organisms spread by aerially dispersed small propagules that exhibit LDD may follow similar dispersal patterns over a several hundred- or thousand-fold expanse of spatial scale. Given that the primary mechanisms driving aerial dispersal remains constant, it may be possible to extrapolate across scales when empirical data are unavailable at a scale of interest.

KEYWORDS
dispersal, epidemiology, long-distance dispersal, modelling, modified power distribution, Puccinia, scaling, SEIR, wheat

## 1 | INTRODUCTION

Scaling, in ecology, is the study of how components or processes of an ecosystem change with another variable (Storch, Marquet, & Brown, 2007). Spatial scaling is the set of changes in ecosystems as a function of the grain or resolution, and the extent of distances being considered (Turner, O'Neill, Gardner, & Milne, 1989). Spatial scaling has been shown to cause significant changes

  

in many ecological dynamics, including the relationship of species diversity to productivity (Chase & Leibold, 2002), population synchrony (Lande, Engen, Sæther, & Fahrig, 1999; Liebhold, Koenig, & Bjørnstad, 2004; Mortelliti, Westgate, Stein, Wood, & Lindenmayer, 2015) and reproduction potential (Mikaberidze, Mundt, & Bonhoeffer, 2014). There has been growing interest in how dispersal varies across multiple spatial scales (Bullock & Nathan, 2008; Cadotte & Fukami, 2005; Mundt, Sackett, Wallace, Cowger, & Dudley, 2009a).

Dispersal of organisms or their propagules is an important component of spatial ecology and epidemiology and can have great impact on population dynamics (Hassell, 2000), in that dispersal can allow species to use spatially disparate resources (Gilbert, 2012), to invade new locations (Clark, Lewis, & Horvath, 2001) and to genetically diversify (Ibrahim, Nichols, & Hewitt, 1996). Mode of dispersal can interact with environmental heterogeneity to influence species co-occurrence (Heino, 2013). The dispersal gradients of organisms with differing modes of dispersal can be best fit by differing functions, for example, with rain-splash dispersed propagules more often being better fit by exponential distributions, and aerially dispersed propagules more often being better fit by inverse-power distributions (Fitt, Gregory†, Todd, McCartney, & Macdonald, 1987). Aerial dispersal of small particles has been described by fat-tailed distributions, often in the form of an inverse power or modified inverse power distribution (Bullock & Clarke, 2000; Devaux, Lavigne, Austerlitz, & Klein, 2006; Reynolds, 2011). Given recent advancements in computational power, probability density functions (PDFs) have been increasingly used to describe dispersal kernels—the set of random draws following a given probability density function describing the proportion of total dispersal at a given distance from a source (Holland, 2010). Unlike fitting the inverse power distribution, these PDFs do not require log-transformation, making them useful in handling data sets containing many zeros, as is expected with count data in the tails of dispersal gradients. Changes in the shape of the dispersal kernel can have significant changes in the speed and rate of acceleration of the population changes of invading organisms such as plant pathogens (Kot, Lewis, Driessche, & den., 1996).

Many organisms are aerially dispersed passively by wind (Bullock & Clarke, 2000; Okubo & Levin, 1989; Rieux et al., 2014). The spatiotemporal dynamics of their populations are greatly affected by the physical processes of air movement, most notably wind speed, direction and turbulence (Aylor, 1990; Novak, Warland, Orchansky, Ketler, & Green, 2000; Shaw, Harwood, Wilkinson, & Elliott, 2006), as well as physical attributes of the particles being dispersed, such as their size, mass and surface roughness (Petroff, Mailliat, Amielh, & Anselmet, 2008), which are in turn affected by landscape and plant architecture (Bohrer, Katul, Nathan, Walko, & Avissar, 2008; Costes, Lauri, Simon, & Andrieu, 2013; Damschen et al., 2014). The complexity of these interacting factors has made direct study challenging. However, examining resulting infections can act as a good proxy for dispersal (Madden, Hughes, & Bosch, 2007; Peay, Schubert, Nguyen, & Bruns, 2012). Examining how wind-dispersed organisms spread across spatial scales can improve our understanding of their populations, and the likelihood of introductions into new regions, which could be of importance for managing the spread of invasive plants or infectious diseases. While aerial dispersal is widely recognized as an important component of ecological population dynamics, measuring it has proven challenging due to the small physical size of many propagules, the large number of propagules produced by a dispersing population, the complexity of physical processes involved and the long distances over which propagules can disperse (Nathan, 2001). Long-distance dispersal (LDD) plays an important role in ecological processes, particularly in disease ecology (Bialozyt, Ziegenhagen, & Petit, 2006; Filipe et al., 2012; Mundt, Sackett, Wallace, Cowger, & Dudley, 2009b; Wingen, Shaw, & Brown, 2013), and changes in the tail of the models describing LDD lead to large changes in the populations they predict (Bullock & Clarke, 2000).

Most empirical dispersal studies are not able to incorporate the entire range of distances of dispersal, as this can be upwards of 500 km for aerially dispersed small propagules (Aylor, 1982). Additionally, local aggregation, which can be indicative of accelerating spread, requires a small spatial scale to accurately measure (Lannou, Soubeyrand, Frezal, & Chadœuf, 2008). Inverse power distributions are theoretically scale independent, in that the shape parameter remains unchanged across scales, with only the constant of proportionality changing (Gisiger, 2001; Marquet et al., 2005), potentially making it possible to fit dispersal gradients across multiple scales using a single function.

We used two rusts of wheat (*Triticum aestivum*), wheat stripe rust, causal agent *Puccinia striiformis* f. sp. *tritici* and stem rust, causal agent *P. graminis* f. sp. *tritici*, as model systems to study dispersal across spatial scales. The primary dispersal gradients of wind-spread propagules have been shown to have a great deal of similarity in shape (Bullock & Clarke, 2000; Chamecki, 2012; Mundt, et al., 2009a; Mundt et al., 2009b). However, very few studies of aerial dispersal in the same host–pathogen system across spatial scales exist. The rust species used here, and many of the most problematic plant pathogens, can be dispersed long distances by wind (Aylor, 2003). Rusts are of great economic importance on cereal crops worldwide (Hovmøller, Yahyaoui, Milus, & Justesen, 2008). Similar rust species are common in many other agroecosystems, as well as in natural systems such as prairies (Mitchell, Tilman, & Groth, 2002) and forests (Sinclair, Lyon, & Johnson, 1987). Repeatable scaling relationships, consistent with inverse power law dispersal, were found for stripe rust and other plant and animal diseases caused by LDD pathogens of divergent taxonomy and at scales ranging over five orders of spatial magnitude, from small field plots to intercontinental spread (Mundt & Sackett, 2012; Mundt et al., 2009b, 2013). In the current study, we compared the primary disease gradients of cereal rust across three spatial scales, with the size of the inoculum source, the size of sampling units and spatial extent of sampling varying in the ratio of 1:60:6,000. Here, we define the primary disease gradient as the number of infections as a function of distance after one generation of spread from the inoculum source, or focus. We then

examined whether the predicted disease spread depended upon the scale at which data were collected to estimate dispersal kernels in simulations among the three sets. We used three approaches to determine whether data collected at one spatial scale could be used to model dispersal at a larger spatial scale. The first approach was to determine if the three data sets obtained over this 6,000-fold range of spatial scale could be fit adequately to a single dispersal kernel. The second approach asked whether simulating epidemic spread at different spatial grain sizes results in similar patterns of spatiotemporal spread. Finally, we determined whether dispersal kernel data obtained at one spatial scale can be used to represent spatiotemporal spread disease spread at a larger spatial scale.

## 2 | MATERIALS AND METHODS

### 2.1 | Field methods

Dispersal kernels of wheat rusts field-wide were estimated from disease gradients emanating from artificially inoculated sources in three sets of investigations at differing spatial scales: We compared empirically derived primary disease gradients of cereal rust across three spatial scales: local (inoculum source and sampling unit = 0.0254 m, spatial extent = 1.52 m) field-wide (inoculum source = 1.52 m, sampling unit = 0.305 m and spatial extent = 91.4 m) and regional (inoculum source and sampling unit = 152 m, spatial extent = 10.5 km) (Figure 1). These terminologies have been used to describe a range of spatial scales previously (Benton, Vickery, & Wilson, 2003; Holland, Birkett, & Southway, 2009; Rounsevell, Annetts, Audsley, Mayr, & Reginster, 2003), but refer generally to the order of single meters, tens to hundreds of meters, and thousands of meters respectively. These studies have been described previously in detail but are summarized below.

The local dispersal study (Farber, Medlock, & Mundt, 2017) was conducted in 6-m radius plots, which were thoroughly inspected prior to inoculation to ensure no sporulating infections. Primary disease gradients (gradients determined after one generation of disease spread from the inoculated source) of stripe rust were conducted in 2012, 2013 and 2014 in commercial wheat fields in Jefferson County, OR. Standard agronomic practices for irrigated commercial wheat were used. The study was conducted on a wheat cultivar that

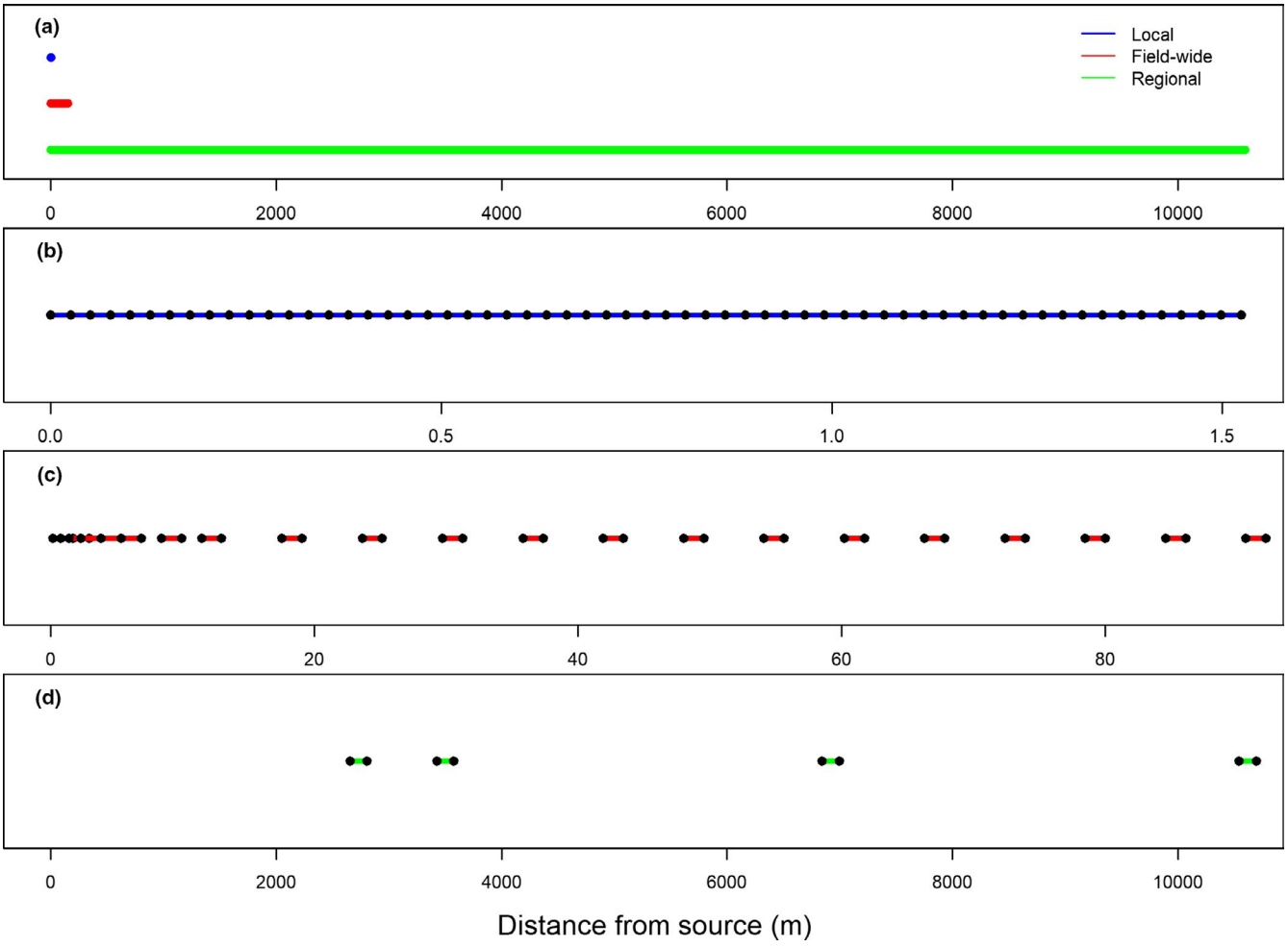


**FIGURE 1** Diagram of the sampling intervals and extents of each dispersal study. (a) Extent of each spatial scale. (b) Detail of the local (Farber et al., 2017) dispersal study, extending to 1.524 m, (c) field-wide (Sackett & Mundt, 2005a) dispersal study, extending to 91.44 m, and (d) regional (Kingsolver et al., 1984) dispersal study, extending to 10.6 km

is highly susceptible to stripe rust and was bordered by a resistant cultivar. The plots were planted in tractor passes 1.52 m wide, each containing seven rows 0.19 m apart. Plant spacing within rows was not controlled but averaged approximately 0.0254 m per plant. A single stripe rust lesion was established by placing a mixture of *P. striiformis* urediniospores and talc on a piece of adhesive tape, which was adhered to the adaxial surface of the uppermost wheat leaf. This plant was then covered with a white plastic bag containing approximately 30 ml of water. The bag and tape were removed approximately 16 hr after inoculation. After 1.2–1.5 latent periods (Shrum, 1975), the plots in which the inoculated leaf contained a sporulating lesion were checked again to ensure no background infection. After 2.75–2.9 latent periods from initial inoculation (1.75–1.9 latent periods of disease spread), the location and number of lesions on each of the non-senesced leaves of all plants within two crossing 3.0 m by 0.3 m transects centred on the inoculated plant were recorded. Plots used for the field-wide primary disease gradient study (Sackett & Mundt, 2005b) were 6.1 m wide and varied in length from 128 to 171 m. Studies were conducted in two semi-arid, irrigated locations in Oregon (Hermiston and Madras) and utilized the same susceptible and resistant varieties as the local dispersal study. An area 1.52 m × 1.52 m in each plot was sprayed with water, inoculated with a 1:10 mixture of *P. striiformis* urediniospores and talc, and covered overnight with plastic. As in the local dispersal study, the success of inoculation and lack of background infections was confirmed visually approximately 1.2 latent periods after inoculation. After approximately 2.5 latent periods, lesions present on a designated leaf of each tiller in two 0.3-m sections of plants was assessed at 0.9, 1.5, 2.1, 3.0, 4.6, 6.1, 9.1 and 12.2 m from the centre of the focus (initial source location), and every 6.1 m further from the focus, assessing a single designated leaf position in a given field and year. While disease severity was assessed in the upwind and downwind directions, only the downwind sites were included in this study.

Long-distance dispersal data unaffected by outside sources of inoculum are extremely difficult to acquire. However, we were able to use stem rust dispersal data from a regional study conducted from 1954 to 1957 on the island of St. Croix in the United States Virgin Islands (Kingsolver, Peet, & Underwood, 1984); only the most complete (1956–1957) field study is used here. Although stripe rust and stem rust are caused by different *Puccinia* species, urediniospores are similar in size, and the epidemiology of the two diseases is very similar (Roelfs, 1989). Despite their respective names, each species can infect both leaves and stems of wheat. Near the northeast edge of the island, a 2.5 ha field of susceptible wheat cultivar Baart was inoculated with *P. graminis*. The prevailing winds are from northeast to southwest. Downwind sites were planted with equal parts of wheat cultivars China and Baart. Fields were routinely checked visually, and once the first rust lesions appeared, 20–30 culms in all downwind locations were surveyed every 2–3 days. Twenty-six days after the initial 2.5 ha focus was inoculated, near the end of the second latent period, rust was observed in the source field (distance = 0) and in four sites downwind at 2.73, 4.34, 6.92 and 10.6 km from the source. Pustules (infections) per culm were recorded in each field when infection levels were below 10. Disease severities (percentage of maximum disease coverage) were estimated at infection densities above 10 pustules per culm. These disease severities were converted to estimated lesion counts by multiplying the severity by the estimated maximum number of lesions within the sampling area.

## 2.2 | Calculation of dispersal kernels

The modified inverse power distribution (Mundt, 1989),

$$y = a * (x + c)^{-b} \quad (1)$$

in which $b$ is the shape of the dispersal gradient, and $a$ is the amount of disease at the source plus $c$, an off-set allowing Equation 1 to be defined for all non-negative numbers, was fit to all dispersal data. $C$ is hypothesized to be related to focus width (Aylor, 1987; Mundt, 1989; Mundt & Leonard, 1985). Equation 1 has been shown to fit aerial dispersal in relatively homogenous environments well, particularly relative to the exponential distribution,

$$y = a * e^{-bx} \quad (2)$$

(Aylor, 1987; Sackett & Mundt, 2005b). This was verified by fitting primary disease gradients combined across the local, field-wide and regional scales as described below to Equation 2. As in previous studies (Brophy & Mundt, 1991; Sackett & Mundt, 2005a) we used the half-width of the inoculated focus for $c$, except for data sets incorporating individual plant data, for which intermingling of plants and plant movement in the wind results in a source size that is difficult to define. For these data sets, the modified inverse-power regression (Equation 1) was fit by iteratively increasing the $c$ value from Equation 1 from $c$ = 0.01 m to 10 m by 0.01 m, and $\log_{10}$-transforming the explanatory variable and the response variable, then fitting them by simple linear regression. The model returning the highest $R^2$ value was considered the best fit when that model was within an order of magnitude of the half-width of the source focus. $c$ was set to the half-width in the spatiotemporal model (see below).

Data sets were combined to predict the number of infections resulting from a single stripe rust lesion over different scales. The local and field-wide data sets were combined by normalizing to the number of lesions for the local data set at 0.914 m, the single distance that was common to both experiments, to account for the differing levels of initial inoculum in the two trials. This was done by calculating the local/field-wide ratio for number of lesions at 0.914 m and multiplying this ratio with the number of lesions at each distance (from 0.914 m to the maximum distance) for each observation in the field-wide data set. Kingsolver et al. (1984) reported pustules per culm at low severities, and severity as a percentage at higher severities describing regional dispersal. The severities were converted to estimates of pustule counts, using their recommendation of 10 pustules = 1% severity. Combining these data with the regional data set was more difficult, as there were no overlapping distances. We thus extrapolated from the local/field-wide combined gradient to predict the number of pustules at the closest diseased sampling

**TABLE 1** Summary of all cereal rust epidemic simulations

| Run | Length of field (m) | Compartment size (m) | $m^2$ | $N^a$ | $f^b$ | DMFR[c] | $P_0{}^d$ |
|---|---|---|---|---|---|---|---|
| 1 | 91.44 | 0.0254 (1×) | 300 | 3,600 | 60 | 5 | 1 |
| 2 | 91.44 | 0.0254 (1×) | 300 | 3,600 | 60 | 2.5 | 1 |
| 3 | 91.44 | 0.0254 (1×) | 300 | 3,600 | 60 | 1 | 1 |
| 4 | 91.44 | 0.0254 (1×) | 300 | 3,600 | 60 | 5 | 5 |
| 5 | 91.44 | 0.0254 (1×) | 300 | 3,600 | 60 | 2.5 | 5 |
| 6 | 91.44 | 0.0254 (1×) | 300 | 3,600 | 60 | 1 | 5 |
| 7 | 91.44 | 0.0254 (1×) | 300 | 3,600 | 60 | 5 | 10 |
| 8 | 91.44 | 0.0254 (1×) | 300 | 3,600 | 60 | 2.5 | 10 |
| 9 | 91.44 | 0.0254 (1×) | 300 | 3,600 | 60 | 1 | 10 |
| 10 | 91.44 | 1.524 (60×) | 1.8E04 | 60 | 1 | 5 | 1 |
| 11 | 91.44 | 1.524 (60×) | 1.8E04 | 60 | 1 | 2.5 | 1 |
| 12 | 91.44 | 1.524 (60×) | 1.8E04 | 60 | 1 | 1 | 1 |
| 13 | 91.44 | 1.524 (60×) | 1.8E04 | 60 | 1 | 5 | 5 |
| 14 | 91.44 | 1.524 (60×) | 1.8E04 | 60 | 1 | 2.5 | 5 |
| 15 | 91.44 | 1.524 (60×) | 1.8E04 | 60 | 1 | 1 | 5 |
| 16 | 91.44 | 1.524 (60×) | 1.8E04 | 60 | 1 | 5 | 10 |
| 17 | 91.44 | 1.524 (60×) | 1.8E04 | 60 | 1 | 2.5 | 10 |
| 18 | 91.44 | 1.524 (60×) | 1.8E04 | 60 | 1 | 1 | 10 |
| 19 | 10,668 | 1.524 (60×) | 1.8E04 | 7,000 | 100 | 5 | 1 |
| 20 | 10,668 | 1.524 (60×) | 1.8E04 | 7,000 | 100 | 2.5 | 1 |
| 21 | 10,668 | 1.524 (60×) | 1.8E04 | 7,000 | 100 | 1 | 1 |
| 22 | 10,668 | 1.524 (60×) | 1.8E04 | 7,000 | 100 | 5 | 5 |
| 23 | 10,668 | 1.524 (60×) | 1.8E04 | 7,000 | 100 | 2.5 | 5 |
| 24 | 10,668 | 1.524 (60×) | 1.8E04 | 7,000 | 100 | 1 | 5 |
| 25 | 10,668 | 1.524 (60×) | 1.8E04 | 7,000 | 100 | 5 | 5 |
| 26 | 10,668 | 1.524 (60×) | 1.8E04 | 7,000 | 100 | 2.5 | 10 |
| 27 | 10,668 | 1.524 (60×) | 1.8E04 | 7,000 | 100 | 1 | 10 |
| 28 | 10,668 | 152.4 (6,000×) | 1.8E06 | 70 | 1 | 5 | 1 |
| 29 | 10,668 | 152.4 (6,000×) | 1.8E06 | 70 | 1 | 2.5 | 1 |
| 30 | 10,668 | 152.4 (6,000×) | 1.8E06 | 70 | 1 | 1 | 1 |
| 31 | 10,668 | 152.4 (6,000×) | 1.8E06 | 70 | 1 | 5 | 5 |
| 32 | 10,668 | 152.4 (6,000×) | 1.8E06 | 70 | 1 | 2.5 | 5 |
| 33 | 10,668 | 152.4 (6,000×) | 1.8E06 | 70 | 1 | 1 | 5 |
| 34 | 10,668 | 152.4 (6,000×) | 1.8E06 | 70 | 1 | 5 | 10 |
| 35 | 10,668 | 152.4 (6,000×) | 1.8E06 | 70 | 1 | 2.5 | 10 |
| 36 | 10,668 | 152.4 (6,000×) | 1.8E06 | 70 | 1 | 1 | 10 |

All simulations were 98 days long, with a latent period and infectious period of 14 days each. Dispersal was governed by the normalized best-fit modified inverse-power distribution across local (0.0254 m), field-wide (1.524 m) and regional (152.4 m) spatial scales, $y = 1.26\,(x + 0.14m)^{-2.39}$.

[a]Number of compartments in simulation.

[b]Number of compartments in focus containing inoculum at the start of the epidemic.

[c]Daily multiplication factor, the number of effective propagules produced by a single lesion per day of the infectious period.

[d]Initial severity within the focus expressed as a percentage.

point outside the focus for the regional data set (2.73 km). The data set was then joined to the others, as described above, by calculating the extrapolated/regional pustule ratio for number of lesions at 2.73 km and multiplying this ratio times the number of lesions at each distance (from 2.73 to 10.6 km) for each observation in the regional data set. A similar extrapolation/normalization was also used

for pairwise combinations of the local with the regional data set, and the field-wide with the regional data set.

## 2.3 | Modelling disease spread

We developed a modified SIR (Kermack William Ogilvy, McKendrick A. G., & Walker Gilbert Thomas, 1927, 1932) model, a susceptible-latent-infectious-removed (SLIR) (Heuer, French, Jackson, & Mackereth, 2007; Pedrazzoli et al., 2017), which addresses similar processes as susceptible-exposed-infected-removed (SEIR) models (Cunniffe, Stutt, Bosch, & Gilligan, 2011; Gilligan & van den Bosch, 2008; Goleniewski, 1996) to examine the spread of epidemics of aerially dispersed pathogens over time. Ours is a deterministic time-step model developed in MATLAB (MATLAB Release, 2016a, 2016), The model is comprised of four interacting arrays representing a one-dimensional field of locations $x$ from 1 to $n$ at all times $t$ from 1 to $T$: $p$, the susceptible, uninfected fraction of each compartment; $u$, the latently infected fraction, with a latent period of $l$ days; $v$, the infectious, actively sporulating fraction, with an infectious period of $d$ days and $w$, the removed fraction, consisting of lesions which have reached the end of their infectious periods and therefore no longer contribute to the epidemic. Here, $s$ represents the incremental day of the latent or infectious period. Each non-zero compartment was assumed to contain $m$ sites available for infection. A factorial design of daily multiplication factor (DMFR), defined as the number of effective spores produced from a single infection during a single day, and a severity of $P_0$ in the focus $x_f$ at $t = 0$ initialized the epidemic simulations (Table 1). At each subsequent time $t$, the fraction of each compartment latently infected was given by the following set of equations:

$$u\left(t+1,x_i,1\right)=\left(\sum_{j=1}^{n}k\left(x_i,x_j\right)r_0v\left(t,x_j\right)\right)\left(m-\sum_{s=1}^{l}u\left(t,x_i\right)-\sum_{s=1}^{d}v\left(t,x_i\right)-w\left(t,x_i\right)\right) \quad (3)$$

for newly arising latent infections, and

$$u\left(t+1,x_i,s+1\right)=u\left(t,x_i,s\right) \quad (4)$$

for all days $s$ from 1 to $l - 1$. The dispersal $k$ from a given source $x_j$ to destination $x_i$ followed the modified inverse power function Equation 1, as a function of the distance from the source $\left|x_j-x_i\right|$ $\left|x_j-x_i\right|$ $r_0$ $r_0$ denotes the DMFR (not to be confused with $R_0$, the number of progeny infections produced by a single source infection over an entire infectious period).

The actively infectious fraction was given by the equations

$$v\left(t+1,x_i,1\right)=u\left(t,x_i,l\right) \quad (5)$$

and

$$v\left(t+1,x_i,j+1\right)=v\left(t,x_i,j\right) \quad (6)$$

for all days $j$ from 1 to $d - 1$. The removed fraction was defined by

$$w\left(t+1,x_i\right)=v\left(t,x_i,d\right) \quad (7)$$

The healthy fraction of each compartment was all tissue not in one of the previous three arrays:

$$p\left(t+1,x_i\right)=m-\sum_{s=1}^{l}u\left(t,x_i\right)-\sum_{s=1}^{d}v\left(t,x_i\right)-w\left(t,x_i\right) \quad (8)$$

## 2.4 | Appropriateness of the dispersal kernel

To demonstrate the ability of the fitted primary dispersal gradient to reproduce empirical data for subsequent generations of disease spread, the Madras 2002 primary disease gradient (Sackett & Mundt, 2005a) was used in the SLIR model with the same initial conditions as in the field. The SLIR model was populated by the dispersal kernel from the regression fit to the primary disease gradient

$$k\left(x_i,x_j\right)=40.5\left(\left|x_i-x_j\right|+0.762\right)^{-2.39} \quad (9)$$

and the initial disease severity in the focus of 6.2% was derived from the Madras 2002 data. The value of 40.5 comes from the regression fit to the primary disease gradient in Sackett & Mundt, 2005a and is the predicted disease severity at 1-c units of distance from the centre of the source. Parameters used previously to model wheat stripe rust spread in (Sackett & Mundt, 2005b) an infectious period of 14 days, a latent period of 17 days, and an $r_0$ of 5 were input to the MATLAB model, considering each compartment to represent a 1.524 m (60x) block of wheat plant with an $m$ of 18,000. The resulting dispersal gradients on the final day of the simulation were fit by the modified inverse power distribution (Equation 1), which returned the proportion of the total effective spores deposited within a given distance from the source. The primary disease gradient from the model was compared to the empirical primary disease gradient at each scale by an analysis of covariance, performing weighted generalized least squares with a dummy variable (Andrade & Estévez-Pérez, 2014).

## 2.5 | Simulating full season epidemics at different spatial scales

The disease gradients were modelled with resolutions and extents with a ratio of 1:60:6,000 representing the local, field-wide and regional scales respectively. The compartment sizes were 0.0254 m (referred to hereafter as 1×), representing the width of an average wheat plant; 1.524 m (referred to hereafter as 60×), the size of the focus used in the field-wide studies and 152.4 m (referred to hereafter as 6,000×), approximately the width of the initially inoculated field in the regional study. Fitting Equation 1 was accomplished by setting the $c$ value, which is likely related to the size of the source, to half the width of the focus (Aylor, 1987; Chamecki, Dufault, & Isard, 2012; Mundt, 1989).

Two sets of epidemics were simulated across host compartments from a single focus to compare the local and field-wide spatial scales, and the field-wide and regional spatial scales. The local and regional spatial scales could not be directly compared due to computational limitations of simulating regional extent with a resolution of 1×. The

length of the epidemic was 98 days, with a latent period and an infectious period of 14 days each. The maximum number of infections *m* in each simulation was scaled based on 300 infections per 1× compartment. A complete factorial of simulations with a range of initial severities ($P_0$) and daily multiplication factor rates (DMFR) were run comparing the 1× resolution to the 60× resolution in field-wide epidemics, and comparing the 60× resolution to the 6,000× resolution in the regional epidemics (Table 1). Figures were produced with MATLAB and in R (R Development Core Team, 2015), including the ggplot2 (Wickham et al., 2013) package. Areas under the curve were approximated using Reimann sums on the last day of the epidemic.

In addition to the simulations governed by the best-fit normalized modified inverse power distribution combined across all spatial scales, full season epidemics were simulated using the non-normalized dispersal kernels from a single spatial scale. Simulations comparing dispersal over 91.44-m fields, as above, were run with dispersal kernels from the local data set, and from the field-wide data set. Simulations comparing dispersal over 10.668-km fields, as above, were run with dispersal kernels from the field-wide data set, and from the regional data set. To examine the sensitivity of the model to changes in the shape parameter of the dispersal gradient, full season epidemics were simulated using a DMFR of 2.5 and a $P_0$ of 0.05, with a *b* of 1.5, 2, 2.39 and 3. Each cell was said to contain plant(s), so *s* was set to 1. A meta-analysis to compare the effect of resolution using the combined-scale dispersal kernel and each individual scale dispersal kernel was conducted. The area under the curve (AUCs) of full season simulations conducted using the 1× and the 60× resolutions with each DMFR and $R_0$ combination was

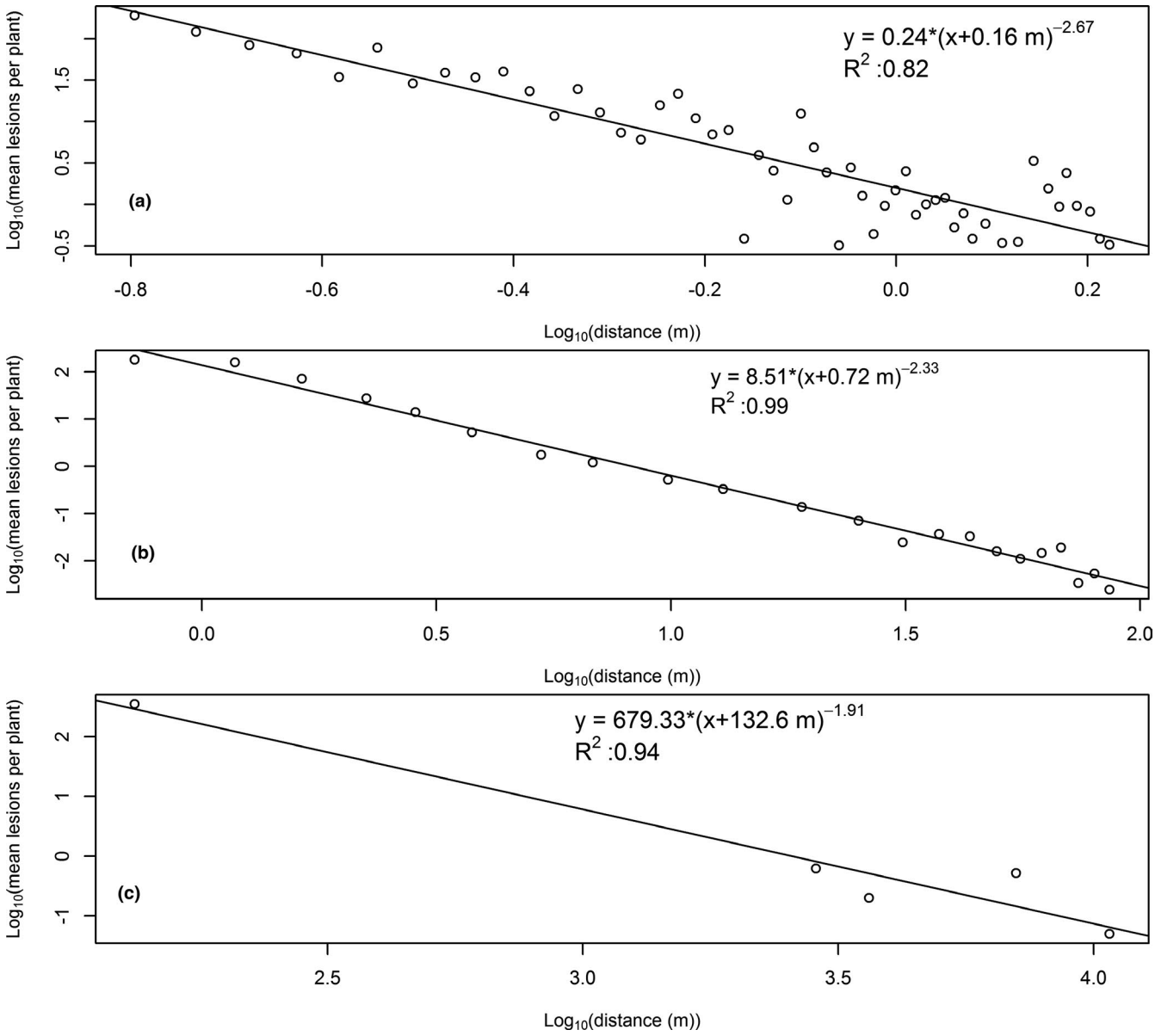


**FIGURE 2** Mean lesion counts of *Puccinia striiformis* f. sp. *tritici* as a function of distance from the source (non-normalized), fit by the modified inverse-power distribution by individual spatial scale data. (a) Local, to 1.52 m; (b) field-wide, to 91.44 m; (c) regional, to 10,668 m

compared, as were the AUCs of full season simulations using the 60× and 6,000× resolutions. The 'linearHypothesis' function from the R package 'Car' (Fox & Weisberg, 2011) was used to compare regression slopes to each other and to 1.

## 3 | RESULTS

The local and field-wide spatial scale data sets were well-fit by the modified inverse power distribution at the local (Figure 2a) and field-wide (Figure 2b) spatial scales. However, the regional data set, containing only four observations in the tail of the epidemic outside the source, was poorly fit by the best-fit *c* modified inverse power distribution, and may have been greatly influenced by an 'outlier' at 3.9 km. Therefore, the regional data set was fit by the modified inverse power distribution with a half-width *c* (Figure 2c). A hierarchical analysis of regression showed that including scale as an additive explanatory variable or as an interaction did not significantly improve fit, suggesting a single function well fit all three spatial scales (Table 2). The normalized local, field-wide and regional data combined in all two-way comparisons (Figure 3a–c) were fitted well by the modified inverse-power distribution, as was the data set combining observations at all three spatial scales (Figure 3d); all four of these data sets were poorly fit by Equation 2, the exponential distribution (Figure S1). The kernel slopes (*b*-values) for these primary disease gradients ranged from 1.91 to 2.69, and values of *c* were proportional to the size of the smallest host unit included in the regression (Figure 3 and Figure S2).

The one-dimensional SLIR model closely recreated the empirical disease spread data. The field-wide primary disease gradient from Madras 2002 was recreated using both 1× (Figure S2a) compartments and 60× compartments (Figure S2b). The model was additionally validated by simulating local and regional primary gradients with the input parameters from the Madras 2002 study conducted at the field-wide scale. The difference in slopes between the simulated primary disease gradient and the empirically derived dispersal gradients were not significant (local *p*-value: 0.14; regional *p*-value: 0.10). The dispersal kernel was governed by the modified inverse-power distribution fit to the combined normalized data across all three spatial scales, setting *c* to the half-width of the compartment size, which when modelling by 1× compartments, was

$$y = 0.23\left(x + 0.0127\,m\right)^{-2.39}, \tag{10}$$

$$y = 0.23\left(x + 0.76\,m\right)^{-2.39} \tag{11}$$

when modelling by 1.524 m compartments, and

$$y = 0.23\left(x + 76.2\,m\right)^{-2.39} \tag{12}$$

when using a compartment size of 6,000×.

Disease spread over time when governed by Equation 10 and Equation 11 was very similar over the course of seven latent periods when comparing compartment sizes of 1× and 60× (Figure 4, Figures S3–S10) across the range of initial severities and reproductive rates per day of the infectious period (DMFR) field-wide. This was evidenced by similar AUCs (Figure 5a) out to 91.44 m. The slope of the regression of the AUCs of the combined-scale dispersal kernel over the field-wide extent (Figure 5a) did not differ significantly from 1 ($p = 0.383$). All other regressions of AUC differed significantly from 1. Additionally, the regressions of the AUCs resulting from the combined-scale dispersal kernel had significantly different slopes than the AUCs resulting from individual scale dispersal kernels ($p < 0.05$). This closeness of AUCs from the full season epidemic simulations across spatial scales also was observed in all combinations of DMFR and $P_0$ using compartment sizes of 60× and 6,000× (Figure 5a, Figures S3–S10) to 10.6 km, governed by Equation 11 and Equation 12. Full season disease simulations governed by Equations 10–12, but with *b* values of 1.5, 2, 2.39 and 3, resulted in very similar levels of disease after seven generations when comparing simulations with resolutions of 1× and 60× (Figure S11) and when comparing simulations with resolutions of 60× and 6,000× (Figure S12). The closeness of simulations using single spatial scale non-normalized dispersal gradients over the course of a full season of disease spread was shown by AUC, although this relationship was not as close as observed using the same normalized combined dispersal kernel as above (Figure 5a and b).

**TABLE 2** A hierarchical analysis of regression, comparing model 1, in which logtransformed distance was the only explanatory variable, to models including scale as an additive explanatory variable (model 2) or as an interaction (model 3)

| | Res.Df | RSS | Df | Sum of Sq | *F* | Pr(>*F*) |
|---|---|---|---|---|---|---|
| 1 | 75 | 11.569 | | | | |
| 2 | 73 | 10.67 | 2 | 0.89899 | 3.097 | 0.05134 |
| 3 | 71 | 10.305 | 2 | 0.36503 | 1.2575 | 0.29062 |

Model 1: log(lesions) ~ log(distance).
Model 2: log(lesions) ~ log(distance) + scale.
Model 3: log(lesions) ~ log(distance) + scale + log(distance):scale.

## 4 | DISCUSSION

Here, we have analysed the only data set examining aerial dispersal across three spatial scales we are aware of, including one of the highest resolution studies of aerial dispersal close to the source, and a study with one of the largest extents. The unique situation provided by these three studies of wheat rusts has demonstrated the similarity of dispersal kernels across a wide range of spatial scales for an aerially dispersed model plant pathogen. We have demonstrated that the primary disease gradients of cereal rust lesion counts are well fitted by the same modified inverse power function at the local, field-wide and regional scales (Figure 3). Using this combined gradient resulted in multi-generation disease spread that was highly similar in simulations of differing resolutions, suggesting that the effect of significantly reducing the resolution (60× comparing field-wide

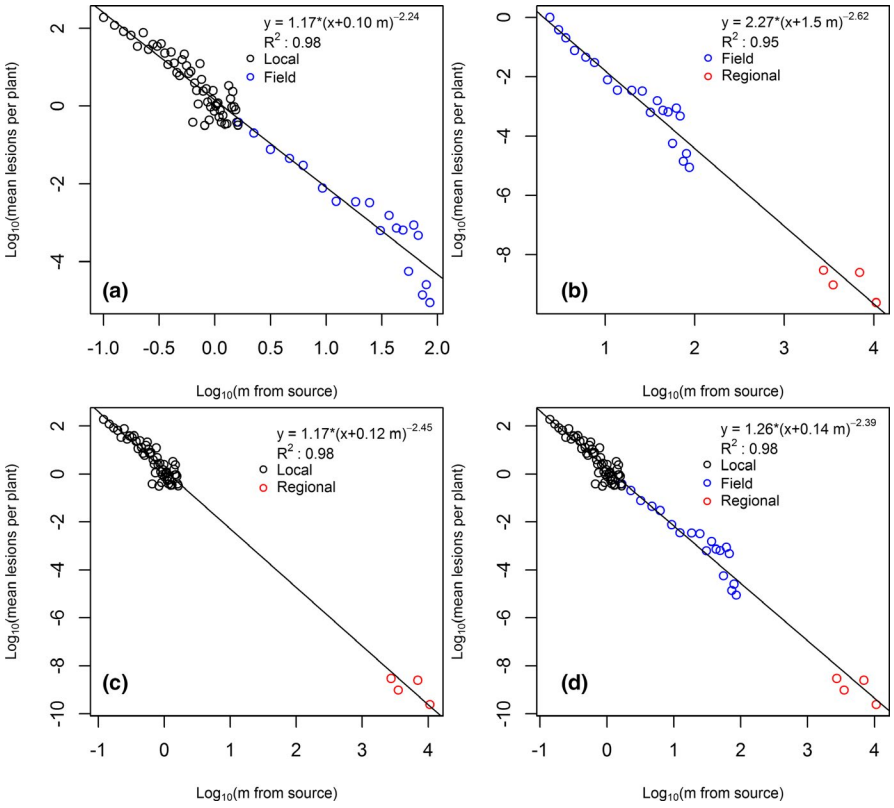


**FIGURE 3** Cereal rust (*Puccinia striiformis* f. sp. *tritici*) at the local and field scales, and *Puccinia graminis* f. sp. *tritici* at the regional scale) best-fit *c* modified inverse power distributions of combined field data normalized to the number of lesions observed or estimated at 0.9144 m. (a) local and field data; (b) field and regional data; (c) local and regional data; (d) local, field, and regional data

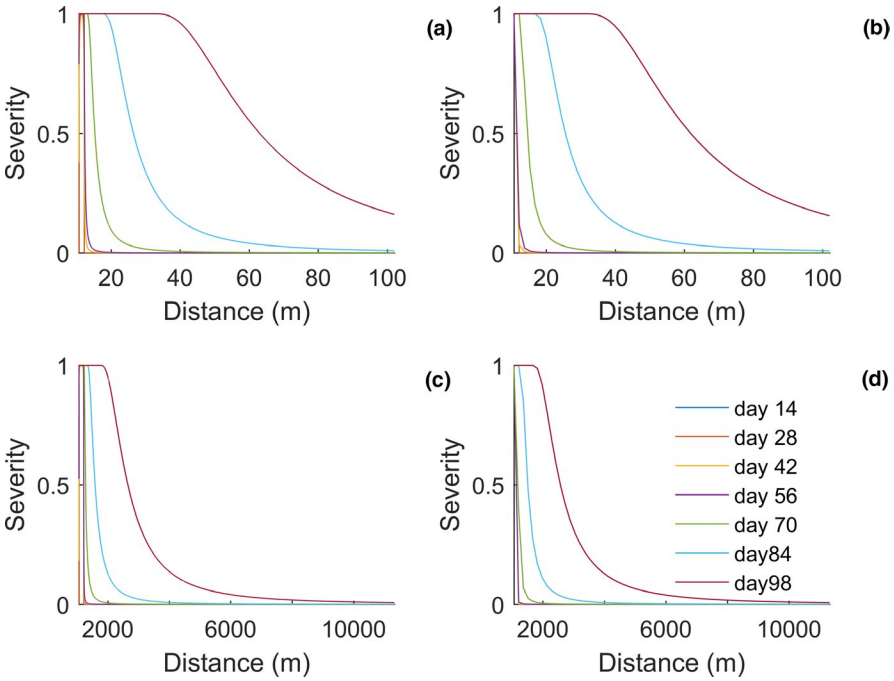


**FIGURE 4** Seven generations of disease spread with a daily multiplication factor (DMFR) of 5 and an initial severity ($P_0$) of 5% from (a and b) a 1.524 m focus across a field extending 105.16 m to the right of the focus, with a compartment size of (a) 0.0254 m and (b) 1.524 m; and from (c and d) a 152.4 m focus across a field extending 10,516 m to the right of the focus with a compartment size of (c) 1.524 m and (d) 152.4 m. Dispersal was governed by the normalized best-fit modified inverse-power distribution across local, field-wide and regional spatial scales, $y = 1.26\,(x+0.14m)^{-2.39}$

simulations and 100× comparing regional simulations) per se did not influence simulated epidemic spread. If modellers can reduce resolution of simulations, that could increase speed of computation by reducing matrix size, which could, therefore, increase feasibility of simulating larger extents. Flexibility of resolution could better align dispersal models with other environmental parameters which may only be available at particular resolutions or spatial grains, as these data may be biased by misaligned resolutions (Sutton & Armsworth, 2014; Tarasi & Peet, 2017). When kernels collected at the local scale were used to simulate epidemic spread at the field-wide spatial scale, epidemics were very similar. When using the field-wide kernel to predict regional spread, a linear relationship was found between epidemic extent, suggesting qualitatively similar patterns, although the rates of spread were dissimilar, with faster predicted spread in

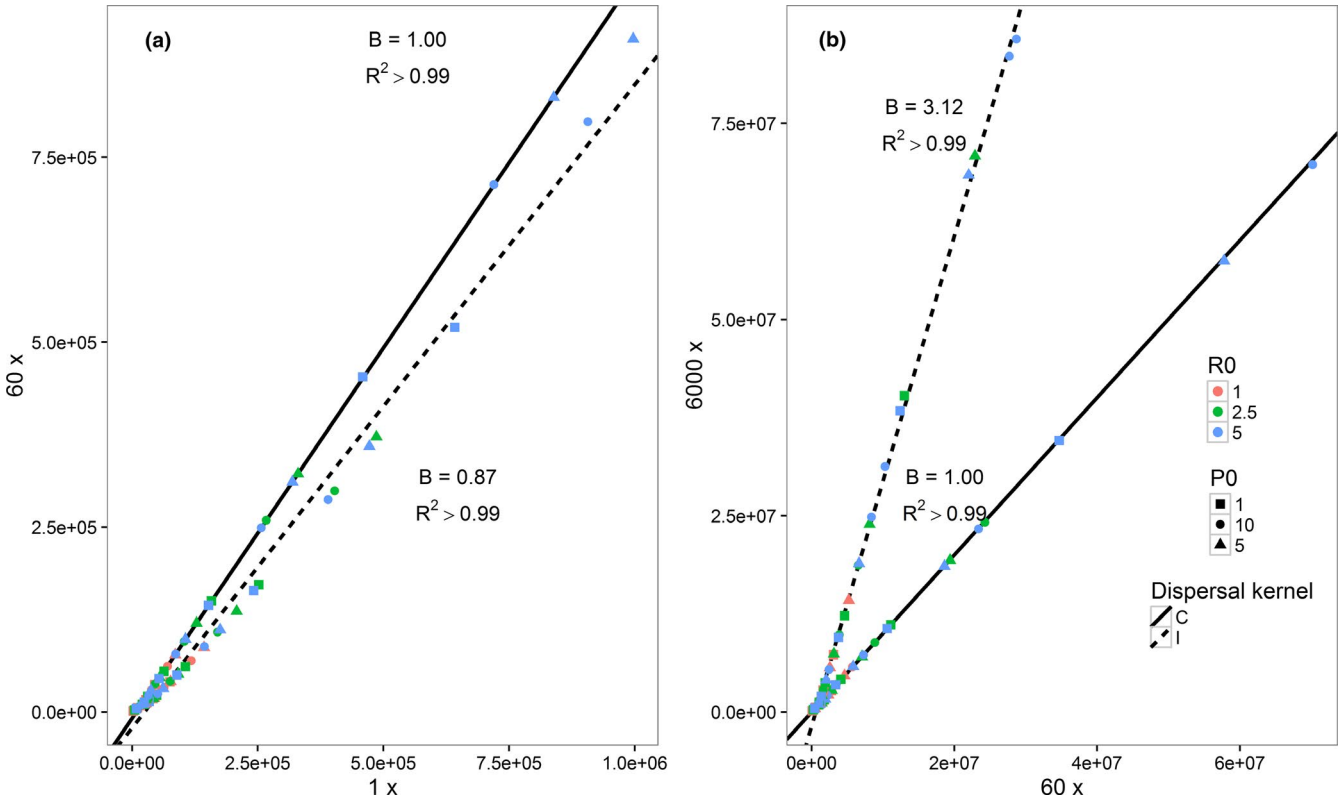


**FIGURE 5** Area under the curve (AUC) calculated for all compartments for all combinations of daily multiplication factor (DMFR) and initial prevalence as a percentage ($P_0$) at the end of latent periods 3–7. (a) 91.44-m field simulation: dispersal was governed by the combined (C; black points) normalized best-fit *c* modified inverse-power distribution across local, field-wide and regional spatial scales, $y=1.26\,(x+0.14m)^{-2.39}$ (slope: 1.00), and the individual spatial scale (I; white points) fixed half-width *c* modified inverse-power distributions, $y=2.46\,(x+0.0127m)^{-2.67}$ and $y=8.51\,(x+0.72m)^{-2.33}$ at the local and field-wide scales respectively (slope: 0.87). (b) 10.6-km field simulation: dispersal was governed by the combined (C; black points) normalized best-fit modified inverse-power distribution across local, field-wide, and regional spatial scales, $y=1.26\,(x+0.14m)^{-2.39}$ (slope: 1.00), and the individual spatial scale (I; white points) fixed half-width *c* modified inverse-power distributions, $y=8.51\,(x+0.72m)^{-2.33}$ and $y=679.33\,(x+132.6m)^{-1.91}$ at the field-wide and regional scales respectively (slope: 3.12).

the simulations using the regional dispersal kernel, possibly owing to the relatively shallow slope of the dispersal gradient measured at the regional scale, which may be either a real effect or a random effect related to the low number of data points present in that study.

As noted by Lannou et al. (2008), large inoculum sources are required to track disease gradients at long distances, but large inoculum sources make it impossible to obtain useful data at short distances. Our results are particularly novel in providing the potential to aid in our ability to understand the dispersal of small, passively wind-dispersed particles by combining data sets to provide a common function across a large spatial extent. We normalized our local and field-level data to sampling at a common distance from the source. As there was no common distance between field-level and regional-level data, the field-level data were extrapolated to the nearest distance from the source in the regional data set for normalization. Although not ideal, this procedure resulted in a linear relationship across the three data sets on the log-transformed scale (Figure 2).

The power law is known to be theoretically scale independent and has been used to model fractal phenomena in which similar processes are repeated across scales (Gisiger, 2001), although this study represents a rare empirical validation of this, particularly as it relates to dispersal. In systems exhibiting significant long-distance dispersal, disease spread has been shown to be driven by dispersal approximating an inverse power law, often with an exponent approximating 2, for both plant and animal systems and over a range of spatial scale (Chis Ster & Ferguson, 2007; Meyer & Held, 2014; Mundt et al., 2009a; Pybus et al., 2012). In other cases, however, the spatial scale at which systems are examined can have significant impacts on dispersal patterns (Bowler & Benton, 2005; Nathan & Muller-Landau, 2000; De Roos, Mccauley, & Wilson, 1991). For example, Kristensen, Barro, and Schellhorn (2013) found that the insect *Eretmocerus hayati* exhibited dispersal which varied with spatial scale and that measuring or modelling its dispersal from solely a local scale would generate observations or predictions of significantly slower dispersal than if the larger spatial scales were included. The rationale given was the differing dominant dispersal mechanisms of *E. hayati* at differing spatial scales, in which diffusion plays a larger role at the local and field-wide scales, but wind-advection was the primary driver of dispersal at the regional scale. This may be the case

for a significant fraction of flying arthropods and may be a significant driver of insect invasions into new regions (Compton, 2002; Wiktelius, 1981).

A challenge in disease ecology has been to predict the probability of pathogen movement to long distances from small sources of inoculum. Use of our combined data (Figure 2) shows that, although a single uredinium could result in disease spread 10 km away, it would be nearly impossible to find even with extensive sampling procedures. Thus, a single infection might be expected to spread to very long distances in an extensively grown agricultural crop. In less extensively grown crops or in sporadic populations of native plants, it is possible that infection would not spread owing to stochastic events. Relatedly, this could predict the number of plants or the area over which one would need to search to find a single progeny lesion at a given distance from a source (Table 3), which could inform field managers of the likelihood of invasions into new fields or regions (Clark et al., 2001).

Due to computational limitations, we used a one-dimensional simulation of disease spread, which functioned well to recreate empirical observations of primary disease gradients. However, a spatially explicit two-dimensional model could offer significant improvements, particularly when compartments lack homogeneity, such as could be the case with row structure or plant architecture heterogeneity (Bohrer et al., 2008; Suzuki & Sasaki, 2011) or anisotropic dispersal (Savage, Barbetti, Macleod, Salam, & Renton, 2011). While the deterministic SIR model has been found to effectively estimate parameters of epidemics with large populations and $R_0$s (Allen & Burgin, 2000; Maltz & Fabricious, 2016), a stochastic model, while significantly more computationally intensive, may confer advantages in its ability to capture rare events (Popinga, Vaughan, Stadler, & Drummond, 2015; Wilkinson, Ball, & Sharkey, 2016). Similarly, a model in which the latent and infectious periods follow an exponential distribution may reduce bias relative to assuming a constant rate (Lloyd, 2001). The position of the epidemic front is expected to increase exponentially over time for an epidemic driven by power law dispersal (Madden et al., 2007; Mundt et al., 2009b), which was observed in our simulations.

Our results suggest dispersal across a range of spatial scales follows similar patterns. This is consistent with previous work with a diversity of plant and animal systems showing that epidemics caused by pathogens dispersed long distance follow similar patterns of disease spread over spatial scales exceeding five orders of magnitude (Mundt et al., 2009a, 2009b; Pybus et al., 2012). While this study provides insights into the scalability of aerial dispersal gradients, further studies examining the scalability at the continental scale of distances upwards of 100 km are needed to extend these findings. Additionally, comparisons of dispersal across spatial scales of propagules with differing physical properties could address the applicability of these findings. Plant pathogens that are dispersed more locally (e.g. by splash and those restricted to the soil environment) would not be expected to show the same relationship to scale. While other ecological processes may have a more complex relationship to scale (Compton, 2002; Lundholm, 2009; Martiny, Eisen, Penn, Allison, & Horner-Devine, 2011; Wiktelius, 1981), long-distance epidemic spread for which dispersal kernels are determined primarily by simple dilution over space may have common and predictable patterns of spread over wide a range of spatial scale.

**TABLE 3** Predicted wheat stripe rust lesions per plant after a single generation of disease spread emanating from a single source lesion, and the area over which one would be expected to search to encounter a single lesion

| Distance (m) | Predicted lesions per plant | Expected number of plants needed to find a single infection | Expected $m^2$ needed to find a single infection |
|---|---|---|---|
| 0 | 15.4 | 0.0649 | 4.19E-05 |
| 0.0254 | 10.3 | 0.0968 | 6.24E-05 |
| 0.0508 | 7.34 | 0.136 | 8.79E-05 |
| 0.1 | 4.24 | 0.236 | 1.52E-04 |
| 0.5 | 0.405 | 2.47 | 1.60E-03 |
| 1 | 0.102 | 9.8 | 6.35E-03 |
| 2 | 0.0225 | 44.5 | 0.0287 |
| 4 | 4.63E-03 | 216 | 0.139 |
| 8 | 9.16E-04 | 1,090 | 0.704 |
| 16 | 1.78E-05 | 5.620E03 | 3.63 |
| 32 | 3.42E-05 | 2.93E04 | 18.9 |
| 64 | 6.53-06 | 1.53E05 | 98.8 |
| 128 | 1.25E-06 | 8.03E05 | 518 |
| 500 | 4.78-08 | 20.9E07 | 1.35E03 |
| 1,000 | 9.08-09 | 1.10E08 | 7.10E04 |
| 2000 | 1.73-09 | 5.79E08 | 3.73E05 |
| 5,000 | 1.93-10 | 5.19E09 | 3,35E06 |
| 10,000 | 3.66E-11 | 27.3E10 | 1.76E07 |

## ACKNOWLEDGEMENTS

The authors acknowledge financial support from the NSF/NIH/USDA/BBSRC Ecology and Evolution of Infectious Disease (EEID) Program through NSF award 052756, NIH award R01GM96685, and USDA-National Institute of Food and Agriculture Award 2015-67013-23818. Additional financial support was provided by NSF-DMS-1411853 and by the Oregon Agricultural Experiment Station. We thank Kathryn Sackett and Dr. Paul Severns for their help in this study.

## AUTHOR CONTRIBUTIONS

Dr. Farber conducted the local dispersal fieldwork, developed the mathematical model, performed the analyses, composed the figures and wrote the manuscript. Dr. De Leenheer contributed to development of the mathematical model and editing the manuscript. Dr. Mundt contributed to editing the manuscript, analysing data, the experimental design of the empirical studies and providing guidance in all aspects of assembling this manuscript.

## ORCID

*Daniel H. Farber* https://orcid.org/0000-0002-5411-8827

## REFERENCES

Allen, L. J. S., & Burgin, A. M. (2000). Comparison of deterministic and stochastic SIS and SIR models in discrete time. *Mathematical Biosciences*, *163*, 1–33. https://doi.org/10.1016/S0025-5564(99)00047-4

Andrade, J. M., & Estévez-Pérez, M. G. (2014). Statistical comparison of the slopes of two regression lines: A tutorial. *Analytica Chimica Acta*, *838*, 1–12. https://doi.org/10.1016/j.aca.2014.04.057

Aylor, D. E. (1982). Long-range transport of tobacco blue mold spores. *Agricultural Meteorology*, *27*, 217–232.

Aylor, D. E. (1987). Deposition gradients of urediniospores of *Puccinia recondita* near a source. *Phytopathology*, *77*, 1442–1448.

Aylor, D. E. (1990). The role of intermittent wind in the dispersal of fungal pathogens. *Annual Review of Phytopathology*, *28*, 73–92. https://doi.org/10.1146/annurev.py.28.090190.000445

Aylor, D. E. (2003). Spread of plant disease on a continental scale: Role of aerial dispersal of pathogens. *Ecology*, *84*, 1989–1997. https://doi.org/10.1890/01-0619

Benton, T. G., Vickery, J. A., & Wilson, J. D. (2003). Farmland biodiversity: Is habitat heterogeneity the key? *Trends in Ecology & Evolution*, *18*, 182–188. https://doi.org/10.1016/S0169-5347(03)00011-9

Bialozyt, R., Ziegenhagen, B., & Petit, R. J. (2006). Contrasting effects of long distance seed dispersal on genetic diversity during range expansion. *Journal of Evolutionary Biology*, *19*, 12–20. https://doi.org/10.1111/j.1420-9101.2005.00995.x

Bohrer, G., Katul, G. G., Nathan, R., Walko, R. L., & Avissar, R. (2008). Effects of canopy heterogeneity, seed abscission and inertia on wind-driven dispersal kernels of tree seeds. *Journal of Ecology*, *96*, 569–580. https://doi.org/10.1111/j.1365-2745.2008.01368.x

Bowler, D. E., & Benton, T. G. (2005). Causes and consequences of animal dispersal strategies: Relating individual behaviour to spatial dynamics. *Biological Reviews*, *80*, 205–225. https://doi.org/10.1017/S1464793104006645

Brophy, L. S., & Mundt, C. C. (1991). Influence of plant spatial patterns on disease dynamics, plant competition, and grain yield in genetically diverse wheat populations. *Agriculture, Ecosystems & Environment*, *35*, 1–12. https://doi.org/10.1016/0167-8809(91)90072-6

Bullock, J. M., & Clarke, R. T. (2000). Long distance seed dispersal by wind: Measuring and modelling the tail of the curve. *Oecologia*, *124*, 506–521. https://doi.org/10.1007/PL00008876

Bullock, J. M., & Nathan, R. (2008). Plant dispersal across multiple scales: Linking models and reality. *Journal of Ecology*, *96*, 567–568. https://doi.org/10.1111/j.1365-2745.2008.01382.x

Cadotte, M. W., & Fukami, T. (2005). Dispersal, spatial scale, and species diversity in a hierarchically structured experimental landscape. *Ecology Letters*, *8*, 548–557. https://doi.org/10.1111/j.1461-0248.2005.00750.x

Chamecki, M. (2012). An analytical model for dispersion of biological particles emitted from area sources: Inclusion of dispersion in the crosswind direction. *Agricultural & Forest Meteorology*, *157*, 30–38. https://doi.org/10.1016/j.agrformet.2012.01.010

Chamecki, M., Dufault, N. S., & Isard, S. A. (2012). Atmospheric dispersion of wheat rust spores: A new theoretical framework to interpret field data and estimate downwind dispersion. *Journal of Applied Meteorology and Climatology*, *51*, 672–685. https://doi.org/10.1175/jamc-d-11-0172.1

Chase, J. M., & Leibold, M. A. (2002). Spatial scale dictates the productivity–biodiversity relationship. *Nature*, *416*, 427–430. https://doi.org/10.1038/416427a

Chis Ster, I., & Ferguson, N. M. (2007). Transmission parameters of the 2001 foot and mouth epidemic in Great Britain. *PLoS ONE*, *2*(6), e502. https://doi.org/10.1371/journal.pone.0000502

Clark, J. S., Lewis, M., & Horvath, L. (2001). Invasion by extremes: Population spread with variation in dispersal and reproduction. *American Naturalist*, *157*, 537–554. https://doi.org/10.1086/319934

Compton, S. (2002). Sailing with the wind: Dispersal by small flying insects. In: *Dispersal Ecology: 42nd Symposium of the British Ecological*. Cambridge, England: Society. Cambridge University Press.

Costes, E., Lauri, P. E., Simon, S., & Andrieu, B. (2013). Plant architecture, its diversity and manipulation in agronomic conditions, in relation with pest and pathogen attacks. *European Journal of Plant Pathology*, *135*, 455–470. https://doi.org/10.1007/s10658-012-0158-3

Cunniffe, N. J., Stutt, R. O. J. H., van den Bosch, F., & Gilligan, C. A. (2011). Time-dependent infectivity and flexible latent and infectious periods in compartmental models of plant disease. *Phytopathology*, *102*, 365–380. https://doi.org/10.1094/PHYTO-12-10-0338

Damschen, E. I., Baker, D. V., Bohrer, G., Nathan, R., Orrock, J. L., Turner, J. R., … Tewksbury, J. J. (2014). How fragmentation and corridors affect wind dynamics and seed dispersal in open habitats. *Proceedings of the National Academy of Sciences*, *111*, 3484–3489. https://doi.org/10.1073/pnas.1308968111

De Roos, A. M., Mccauley, E., & Wilson, W. G. (1991). Mobility versus density-limited predator–prey dynamics on different spatial scales. *Proceedings of the Royal Society of London. Series B: Biological Sciences*, *246*, 117–122.

Devaux, C., Lavigne, C., Austerlitz, F., & Klein, E. K. (2006). Modelling and estimating pollen movement in oilseed rape (*Brassica napus*) at the landscape scale using genetic markers: Landscape oilseed rape pollination. *Molecular Ecology*, *16*, 487–499.

Farber, D. H., Medlock, J., & Mundt, C. C. (2017). Local dispersal of *Puccinia striiformis* f. sp. *tritici* from isolated source lesions. *Plant Pathology*, *66*, 28–37.

Filipe, J. A. N., Cobb, R. C., Meentemeyer, R. K., Lee, C. A., Valachovic, Y. S., Cook, A. R., … Gilligan, C. A. (2012). Landscape epidemiology and control of pathogens with cryptic and long-distance dispersal: Sudden oak death in northern Californian forests. *PLoS Computational Biology*, *8*, e1002328. https://doi.org/10.1371/journal.pcbi.1002328

Fitt, B. D. L., Gregory†, P. H., Todd, A. D., McCartney, H. A., & Macdonald, O. C. (1987). Spore dispersal and plant disease gradients; a comparison between two empirical models. *Journal of Phytopathology*, *118*, 227–242. https://doi.org/10.1111/j.1439-0434.1987.tb00452.x

Fox, J., & Weisberg, S. (2011). *An R companion to applied regression (Version 2)*. Retrieved from http://socserv.socsci.mcmaster.ca/jfox/Books/Companion.

Gilbert, B. (2012). Joint consequences of dispersal and niche overlap on local diversity and resource use. *Journal of Ecology*, *100*, 287–296. https://doi.org/10.1111/j.1365-2745.2011.01908.x

Gilligan, C. A., & van den Bosch, F. (2008). Epidemiological models for invasion and persistence of pathogens. *Annual Review of Phytopathology*, *46*, 385–418. https://doi.org/10.1146/annurev.phyto.45.062806.094357

Gisiger, T. (2001). Scale invariance in biology: Coincidence or footprint of a universal mechanism? *Biological Reviews*, *76*, 161–209. https://doi.org/10.1017/S1464793101005607

Goleniewski, G. (1996). Modelling cultivar mixtures using SEIR compartmental models. *Biometrical Journal*, *38*, 281–297. https://doi.org/10.1002/bimj.4710380305

Hassell, M. P. (2000). Host–parasitoid population dynamics. *Journal of Animal Ecology*, *69*, 543–566.

Heino, J. (2013). Environmental heterogeneity, dispersal mode, and co-occurrence in stream macroinvertebrates. *Ecology and Evolution*, *3*, 344–355. https://doi.org/10.1002/ece3.470

Heuer, C., French, N., Jackson, R., & Mackereth, G. (2007). Application of modelling to determine the absence of foot-and-mouth disease in the face of a suspected incursion. *New Zealand Veterinary Journal*, *55*, 289–296. https://doi.org/10.1080/00480169.2007.36783

Holland, J. D. (2010). Dispersal kernel determines symmetry of spread and geographical range for an insect. *International Journal of Ecology*, *2009*, 1–4. https://doi.org/10.1155/2009/167278

Holland, J. M., Birkett, T., & Southway, S. (2009). Contrasting the farm-scale spatio-temporal dynamics of boundary and field overwintering predatory beetles in arable crops. *BioControl*, *54*, 19–33. https://doi.org/10.1007/s10526-008-9152-2

Hovmøller, M. S., Yahyaoui, A. H., Milus, E. A., & Justesen, A. F. (2008). Rapid global spread of two aggressive strains of a wheat rust fungus. *Molecular Ecology*, *17*, 3818–3826. https://doi.org/10.1111/j.1365-294X.2008.03886.x

Ibrahim, K. M., Nichols, R. A., & Hewitt, G. M. (1996). Spatial patterns of genetic variation generated by different forms of dispersal during range expansion. *Heredity*, *77*, 282–291. https://doi.org/10.1038/hdy.1996.142

Kingsolver, C. H., Peet, C. E., & Underwood, J. F. (1984). *Measurement of the epidemiologic potential of wheat stem rust* (pp. 1954–1957). St. Croix, U.S. Virgin Islands: the International System for Agricultural Science and Technology (AGRIS).

Kot, M., Lewis, M. A., & van den Driessche, P. (1996). Dispersal data and the spread of invading organisms. *Ecology*, *77*, 2027–2042. https://doi.org/10.2307/2265698

Kristensen, N. P., Barro, P. J. D., & Schellhorn, N. A. (2013). The initial dispersal and spread of an intentional invader at three spatial scales. *PLoS ONE*, *8*, 1–12. https://doi.org/10.1371/journal.pone.0062407

Lande, R., Engen, S., Sæther, B., & Fahrig, A. E. L. (1999). Spatial scale of population synchrony: Environmental correlation versus dispersal and density regulation. *American Naturalist*, *154*, 271–281. https://doi.org/10.1086/303240

Lannou, C., Soubeyrand, S., Frezal, L., & Chadœuf, J. (2008). Autoinfection in wheat leaf rust epidemics. *New Phytologist*, *177*, 1001–1011. https://doi.org/10.1111/j.1469-8137.2007.02337.x

Liebhold, A., Koenig, W. D., & Bjørnstad, O. N. (2004). Spatial synchrony in population dynamics. *Annual Review of Ecology Evolution and Systematics*, *35*, 467–490. https://doi.org/10.1146/annurev.ecolsys.34.011802.132516

Lloyd, A. L. (2001). Realistic distributions of infectious periods in epidemic models: Changing patterns of persistence and dynamics. *Theoretical Population Biology*, *60*, 59–71. https://doi.org/10.1006/tpbi.2001.1525

Lundholm, J. T. (2009). Plant species diversity and environmental heterogeneity: Spatial scale and competing hypotheses. *Journal of Vegetation Science*, *20*, 377–391.

Madden, L. V., Hughes, G., & van den Bosch, F. (2007). *The study of plant disease epidemics*. St. Paul: American Phytopathological Society.

Maltz, A., & Fabricius, G. (2016). SIR model with local and global infective contacts: A deterministic approach and applications. *Theoretical Population Biology*, *112*, 70–79. https://doi.org/10.1016/j.tpb.2016.08.003

Marquet, P. A., Quiñones, R. A., Abades, S., Labra, F., Tognelli, M., Arim, M., & Rivadeneira, M. (2005). Scaling and power-laws in ecological systems. *Journal of Experimental Biology*, *208*, 1749–1769.

Martiny, J. B. H., Eisen, J. A., Penn, K., Allison, S. D., & Horner-Devine, M. C. (2011). Drivers of bacterial β-diversity depend on spatial scale. *Proceedings of the National Academy of Sciences*, *108*, 7850–7854.

*MATLAB Release 2016a*. (2016). Natick, MA: The Mathworks, Inc.

Meyer, S., & Held, L. (2014). Power-law models for infectious disease spread. *The Annals of Applied Statistics*, *8*, 1612–1639. https://doi.org/10.1214/14-AOAS743

Mikaberidze, A., Mundt, C. C., & Bonhoeffer, S. (2014). The effect of spatial scales on the reproductive fitness of plant pathogens. Arxiv14100587 Q-Bio. https://arxiv.org/abs/1410.0587.

Mitchell, C. E., Tilman, D., & Groth, J. V. (2002). Effects of grassland plant species diversity, abundance, and composition on foliar fungal disease. *Ecology*, *83*(6), 1713–1726.

Mortelliti, A., Westgate, M., Stein, J., Wood, J., & Lindenmayer, D. B. (2015). Ecological and spatial drivers of population synchrony in bird assemblages. *Basic and Applied Ecology*, *16*, 269–278. https://doi.org/10.1016/j.baae.2015.01.008

Mundt, C. C. (1989). Use of the modified Gregory model to describe primary disease gradients of wheat leaf rust produced from area sources of inoculum. *Phytopathology*, *79*, 241–246. https://doi.org/10.1094/Phyto-79-241

Mundt, C. C., & Leonard, K. J. (1985). A modification of gregory's model for describing plant disease gradients. *Phytopathology*, *75*, 930–935. https://doi.org/10.1094/Phyto-75-930

Mundt, C. C., & Sackett, K. E. (2012). Spatial scaling relationships for spread of disease caused by a wind-dispersed plant pathogen. *Ecosphere*, *3*, art24. https://doi.org/10.1890/ES11-00281.1

Mundt, C. C., Sackett, K. E., Wallace, L. D., Cowger, C., & Dudley, J. P. (2009a). Aerial dispersal and multiple-scale spread of epidemic disease. *EcoHealth*, *6*, 546–552. https://doi.org/10.1007/s10393-009-0251-z

Mundt, C. C., Sackett, K. E., Wallace, L. D., Cowger, C., & Dudley, J. P. (2009b). Long-distance dispersal and accelerating waves of disease: Empirical relationships. *American Naturalist*, *173*, 456–466. https://doi.org/10.1086/597220

Mundt, C. C., Wallace, L. D., Allen, T. W., Hollier, C. A., Kemerait, R. C., & Sikora, E. J. (2013). Initial epidemic area is strongly associated with the yearly extent of soybean rust spread in North America. *Biological Invasions*, *15*, 1431–1438. https://doi.org/10.1007/s10530-012-0381-z

Nathan, R. (2001). The challenges of studying dispersal. *Trends in Ecology & Evolution*, *16*, 481–483. https://doi.org/10.1016/S0169-5347(01)02272-8

Nathan, R., & Muller-Landau, H. C. (2000). Spatial patterns of seed dispersal, their determinants and consequences for recruitment. *Trends in Ecology & Evolution*, *15*, 278–285. https://doi.org/10.1016/S0169-5347(00)01874-7

Novak, M. D., Warland, J. S., Orchansky, A. L., Ketler, R., & Green, S. (2000). Wind tunnel and field measurements of turbulent flow in forests. Part I: Uniformly thinned stands. *Boundary-Layer Meteorology*, *95*, 457–495. https://doi.org/10.1023/A:1002693625637

Ogilvy, K. W., McKendrick, A. G., & Thomas, W. G. (1927). A contribution to the mathematical theory of epidemics. *Proceedings of the Royal Society of London. Series A, Containing Papers of a Mathematical and Physical Character*, *115*(772), 700–721.

Ogilvy, K. W., McKendrick, A. G., & Thomas, W. G. (1932). Contributions to the mathematical theory of epidemics. II. The problem of endemicity. *Proceedings of the Royal Society of London. Series A, Containing Papers of a Mathematical and Physical Character*, *138*, 55–83.

Okubo, A., & Levin, S. A. (1989). A theoretical framework for data analysis of wind dispersal of seeds and pollen. *Ecology*, *70*, 329–338. https://doi.org/10.2307/1937537

Peay, K. G., Schubert, M. G., Nguyen, N. H., & Bruns, T. D. (2012). Measuring ectomycorrhizal fungal dispersal: Macroecological patterns driven by microscopic propagules. *Molecular Ecology*, *21*, 4122–4136. https://doi.org/10.1111/j.1365-294X.2012.05666.x

Pedrazzoli, D., Boccia, D., Dodd, P. J., Lönnroth, K., Dowdy, D. W., Siroka, A., … Houben, R. M. G. J. (2017). Modelling the social and structural determinants of tuberculosis: Opportunities and challenges. *The International Journal of Tuberculosis and Lung Disease*, *21*, 957–964. https://doi.org/10.5588/ijtld.16.0906

Petroff, A., Mailliat, A., Amielh, M., & Anselmet, F. (2008). Aerosol dry deposition on vegetative canopies. Part I: Review of present knowledge. *Atmospheric Environment*, *42*, 3625–3653. https://doi.org/10.1016/j.atmosenv.2007.09.043

Popinga, A., Vaughan, T., Stadler, T., & Drummond, A. J. (2015). Inferring epidemiological dynamics with bayesian coalescent inference: The merits of deterministic and stochastic models. *Genetics*, *199*, 595–607. https://doi.org/10.1534/genetics.114.172791

Pybus, O. G., Suchard, M. A., Lemey, P., Bernardin, F. J., Rambaut, A., Crawford, F. W., … Delwart, E. L. (2012). Unifying the spatial epidemiology and molecular evolution of emerging epidemics. *Proceedings of the National Academy of Sciences*, *109*, 15066–15071. https://doi.org/10.1073/pnas.1206598109

R Development Core Team. (2015). *R: A language and environment for statistical computing*. Vienna, Austria: R Foundation for Statistical Computing.

Reynolds, A. M. (2011). Exponential and power-law contact distributions represent different atmospheric conditions. *Phytopathology*, *101*, 1465–1470. https://doi.org/10.1094/PHYTO-01-11-0001

Rieux, A., Soubeyrand, S., Bonnot, F., Klein, E. K., Ngando, J. E., Mehl, A., … de Lapeyre de Bellaire, L. (2014). Long-distance wind-dispersal of spores in a fungal plant pathogen: Estimation of anisotropic dispersal kernels from an extensive field experiment. *PLoS ONE*, *9*, e103225. https://doi.org/10.1371/journal.pone.0103225

Roelfs, A. P. (1989). Epidemiology of the cereal rusts in North America. *Canadian Journal of Plant Pathology*, *11*, 86–90. https://doi.org/10.1080/07060668909501153

Rounsevell, M. D., Annetts, J. E., Audsley, E., Mayr, T., & Reginster, I. (2003). Modelling the spatial distribution of agricultural land use at the regional scale. *Agriculture, Ecosystems and Environment*, *95*, 465–479. https://doi.org/10.1016/S0167-8809(02)00217-7

Sackett, K. E., & Mundt, C. C. (2005a). Primary disease gradients of wheat stripe rust in large field plots. *Phytopathology*, *95*, 983–991. https://doi.org/10.1094/PHYTO-95-0983

Sackett, K. E., & Mundt, C. C. (2005b). The effects of dispersal gradient and pathogen life cycle components on epidemic velocity in computer simulations. *Phytopathology*, *95*, 992–1000. https://doi.org/10.1094/PHYTO-95-0992

Savage, D., Barbetti, M. J., Macleod, W. J., Salam, M. U., & Renton, M. (2011). Can mechanistically parameterised, anisotropic dispersal kernels provide a reliable estimate of wind-assisted dispersal? *Ecological Modelling*, *222*, 1673–1682. https://doi.org/10.1016/j.ecolmodel.2011.03.003

Shaw, M. W., Harwood, T. D., Wilkinson, M. J., & Elliott, L. (2006). Assembling spatially explicit landscape models of pollen and spore dispersal by wind for risk assessment. *Proceedings of the Royal Society B: Biological Sciences*, *273*, 1705–1713. https://doi.org/10.1098/rspb.2006.3491

Shrum, R. (1975). *Simulation of Wheat Stripe Rust (Puccinia striiformis West.) Using Epidemic, a flexible plant disease simulator. Pennsylvania Agri. Exp. Station Progress Report*. University Park, PA. Pennsylvania State University, Agricultural Experiment Station.

Sinclair, W. A., Lyon, H., & Johnson, W. T. (1987). *Diseases of trees and shrubs*. New York, NY: Cornell University Press.

Storch, D., Marquet, P. A., & Brown, J. H. (2007). *Scaling biodiversity (Ecological reviews)*. Cambridge, UK: Cambridge University Press.

Sutton, N. J., & Armsworth, P. R. (2014). The grain of spatially referenced economic cost and biodiversity benefit data and the effectiveness of a cost targeting strategy. *Conservation Biology*, *28*(6), 1451–1461. https://doi.org/10.1111/cobi.12405

Suzuki, S. U., & Sasaki, A. (2011). How does the resistance threshold in spatially explicit epidemic dynamics depend on the basic reproductive ratio and spatial correlation of crop genotypes? *Journal of Theoretical Biology*, *276*, 117–125. https://doi.org/10.1016/j.jtbi.2011.02.002

Tarasi, D. D., & Peet, R. K. (2017). The native-exotic species richness relationship varies with spatial grain of measurement and environmental conditions. *Ecology*, *98*(12), 3086–3095. https://doi.org/10.1002/ecy.2028

Turner, M. G., O'Neill, R. V., Gardner, R. H., & Milne, B. T. (1989). Effects of changing spatial scale on the analysis of landscape pattern. *Landscape Ecology*, *3*, 153–162. https://doi.org/10.1007/BF00131534

Wickham, H., Chang, W., & Wickham, M. H. (2013). Package "ggplot2".

Wiktelius, S. (1981). Wind dispersal of insects. *Grana*, *20*, 205–207. https://doi.org/10.1080/00173138109427667

Wilkinson, R. R., Ball, F. G., & Sharkey, K. J. (2016). The deterministic Kermack-McKendrick model bounds the general stochastic epidemic. *Journal of Applied Probability*, *53*, 1031–1040. https://doi.org/10.1017/jpr.2016.62

Wingen, L. U., Shaw, M. W., & Brown, J. K. M. (2013). Long-distance dispersal and its influence on adaptation to host resistance in a heterogeneous landscape. *Plant Pathology*, *62*, 9–20. https://doi.org/10.1111/j.1365-3059.2012.02621.x

## BIOSKETCHES

This work stemmed from the final chapter of Dr. Farber's Ph.D. dissertation, 'The Primary Disease Gradient of Wheat Stripe Rust (*Puccinia striiformis* f. sp. *tritici*) Across Spatial Scales'. Dr. Farber is currently investigating the epidemiology of potato diseases, and quantifying and modelling the dispersal of *Phytopthora infestans*. **Dr. Mundt** is a disease ecologist and epidemiologist, working to bridge theoretical and applied plant pathology by developing our knowledge of invasion ecology and the factors which exacerbate plant disease epidemics, using cereal pathology as a model. **Dr. De Leenheer** is a mathematician and ecologist with a long track record of modelling growth of biological systems.

## SUPPORTING INFORMATION

Additional supporting information may be found online in the Supporting Information section at the end of the article.

**How to cite this article:** Farber DH, De Leenheer P, Mundt CC. Dispersal kernels may be scalable: Implications from a plant pathogen. *J Biogeogr.* 2019;46:2042–2055. https://doi.org/10.1111/jbi.13642